frontiers in Aging Neuroscience

REVIEW
published: 27 November 2018
doi: 10.3389/fnagi.2018.00394

In vivo X-Nuclear MRS Imaging Methods for Quantitative Assessment of Neuroenergetic Biomarkers in Studying Brain Function and Aging

*Xiao-Hong Zhu * and Wei Chen **

Center for Magnetic Resonance Research (CMRR), Department of Radiology, School of Medicine, University of Minnesota, Minneapolis, MN, United States

Brain relies on glucose and oxygen metabolisms to generate biochemical energy in the form of adenosine triphosphate (ATP) for supporting electrophysiological activities and neural signaling under resting or working state. Aging is associated with declined mitochondrial functionality and decreased cerebral energy metabolism, and thus, is a major risk factor in developing neurodegenerative diseases including Alzheimer's disease (AD). However, there is an unmet need in the development of novel neuroimaging tools and sensitive biomarkers for detecting abnormal energy metabolism and impaired mitochondrial function, especially in an early stage of the neurodegenerative diseases. Recent advancements in developing multimodal high-field *in vivo* X-nuclear (e.g., ^{2}H, ^{17}O and ^{31}P) MRS imaging techniques have shown promise for quantitative and noninvasive measurement of fundamental cerebral metabolic rates of glucose and oxygen consumption, ATP production as well as nicotinamide adenine dinucleotide (NAD) redox state in preclinical animal and human brains. These metabolic neuroimaging measurements could provide new insights and quantitative bioenergetic markers associated with aging processing and neurodegeneration and can therefore be employed to monitor disease progression and/or determine effectiveness of therapeutic intervention.

Keywords: *in vivo* X-nuclear MRS imaging, brain energy metabolism, neuroenergetics, mitochondrial function, ultra-high magnetic field (UHF), aging, neurodegeneration

OPEN ACCESS

Edited by:
Ai-Ling Lin,
University of Kentucky, United States

Reviewed by:
Anant Bahadur Patel,
Centre for Cellular and Molecular Biology (CSIR), India
Basavaraju G. Sanganahalli,
Yale University, United States

****Correspondence:***
Xiao-Hong Zhu
zhu@cmrr.umn.edu
Wei Chen
wei@cmrr.umn.edu

Received: *23 July 2018*
Accepted: *13 November 2018*
Published: *27 November 2018*

Citation:
Zhu X-H and Chen W (2018) In vivo X-Nuclear MRS Imaging Methods for Quantitative Assessment of Neuroenergetic Biomarkers in Studying Brain Function and Aging. Front. Aging Neurosci. 10:394. doi: 10.3389/fnagi.2018.00394

MITOCHONDRIAL DYSFUNCTION AND NEUROENERGETIC DEFICIENCY AS HALLMARKS OF AGING AND NEURODEGENERATION

Aging is an inevitable process of life. With the rapid growth of the elderly population, brain diseases associated with functional decline and neurodegeneration, such as cognitive impairment (CI), Alzheimer's disease (AD) and Parkinson's disease (PD), not only have a huge impact on people's quality of life, but also greatly increase the social and economic burdens. As a complex biological process, aging (defined as an age-progressive decline in intrinsic physiological function) can be influenced by many factors other than the actual age, such as heredity, lifestyle, income and living environment.

Mitochondria are organelles found in the cells of complex organism and they produce >90% of the adenosine triphosphate (ATP) energy molecules in the brain via the oxidative phosphorylation of adenosine diphosphate (ADP). In addition to supporting unceasing neuronal activity, neurotransmission, cellular signaling and other functions under different brain states, approximately one-quarter of total ATP energy expenditure in the human brain is used for biosynthesis and "housekeeping" functions to maintain cellular integrity (Siesjo, 1978; Erecińska and Silver, 1989; Barinaga, 1997; Rolfe and Brown, 1997; Boyer, 1999; Attwell and Laughlin, 2001; Shulman et al., 2004; Hyder et al., 2006; Du et al., 2008; Zhu et al., 2015a). A coupling relationship between the neuronal activity and ATP energy consumption of the brain tissue holds for a wide range of physiological conditions and brain relies on an effective metabolic regulation to balance the ATP supply and demand through key biochemical reactions associated with energy metabolism (Du et al., 2008; Zhu et al., 2012, 2018). Under normal circumstances, the mitochondrial ATP production rate in the brain is indirectly but closely coupled with the cerebral metabolic rates of glucose (CMR_{Glc}) and oxygen ($CMRO_2$) and tightly regulated by the nicotinamide adenine dinucleotide (NAD) redox state, which can be determined by the intracellular concentration ratio of the oxidized (NAD^+) and reduced (NADH) NAD molecules (i.e., NAD redox ratio: RX_{NAD}).

As depicted in **Figure 1**, the circulating blood flow constantly supplies oxygen and glucose to the brain tissue, where the glucose is transported into the brain cells and converted to pyruvate via glycolysis and produces two ATP and two NADH molecules from each glucose molecule consumed in the cytosol. Most pyruvate molecules enter the mitochondria to form acetyl Co-A, its oxidation via the tricarboxylic acid (TCA) cycle produces eight NADH molecules that can be converted to NAD^+ molecules through oxygen metabolism (Stryer, 1988). The electron transport chain reactions extrude H^+ ions from mitochondria to generate an electrochemical potential gradient across the mitochondrial inner membrane, which is the driving force for the mitochondrial F_1F_0-ATP_{ase} mediated enzyme reaction that synthesizes ATP from ADP and inorganic phosphate (Pi; producing >30 ATPs per consumed glucose under physiological condition) and transports the H^+ ions back into mitochondria (Siesjo, 1978; Hyder et al., 2006). The ATP utilization occurs in the cytosol via the ATP hydrolysis reaction. The majority of the ATP energy are used to maintain the Na^+/K^+ ion gradients across the cell membrane for supporting action potential propagation, neuronal firing and neurotransmitter cycling (Siesjo, 1978; Stryer, 1988; Shulman et al., 1999). The rapid ATP turnover requires efficient transportation of the ATP molecules between the cytosolic and mitochondrial compartments to maintain the intracellular ATP homeostasis. This is accomplished partly by a creatine kinase (CK) catalyzed near-equilibrium chemical exchange between ATP + Creatine (Cr) and phosphocreatine (PCr) + ADP (Kemp, 2000; Du et al., 2008).

Although it only accounts for 2% of the total body weight, the human brain has enormous energy needs. The resting adult brain receives approximately 15% of the cardiac output and uses most (∼20%) of systemic oxygen and glucose consumptions (Raichle, 1987; Shulman et al., 2004; Hyder et al., 2006). It is worth noting that the intracellular ATP concentration in the brain is very low (∼3 mM); the entire human brain only contains approximately 2 g of ATP (assuming an average adult brain weight of 1.4 kg). In contrast, the rate of ATP synthesis by the F_1F_0-ATP_{ase} reaction is very high (8–9 μmole/g/min) in the human brain (Lei et al., 2003a; Du et al., 2007; Zhu et al., 2012), indicating that a human brain produces 7–8 kg of ATP molecules (about 5–6 times of the human brain weight) in 1 day. The extreme high turnover between the ATP production and utilization is critical in fulfilling the high energy demand of the neuronal cells and maintaining the intracellular ATP homeostasis.

The conversion between NAD^+ and NADH through the NAD redox reaction determines the intracellular NAD redox state, which controls the balance of cytosolic glycolysis and mitochondrial oxidative phosphorylation to produce adequate ATP molecules (Chance et al., 1962; Lu et al., 2014b; Zhu et al., 2015b). Mitochondrial dysfunction and energy deficiency are the key cellular hallmarks of aging and neurodegeneration, suggesting that mitochondria can serve as therapeutic targets for various neurodegenerative diseases or for monitoring the aging processes (Creasey and Rapoport, 1985; Rapoport, 1999; Balaban et al., 2005; Guarente, 2008; Yap et al., 2009; Reddy and Reddy, 2011; Nunnari and Suomalainen, 2012; López-Otín et al., 2013; Pathak et al., 2013; Lin et al., 2014; Yin et al., 2014). Therefore, the development of quantitative, reliable and sensitive neuroimaging tools or biomarkers capable of assessing mitochondrial function and cerebral energy metabolism is essential for studying the underlying mechanisms of human brain aging and monitoring the progression of aging-related brain disorders. Furthermore, biomarkers with improved specificity and sensitivity can be potentially used to distinguish normal aging from neurodegeneration, provide early diagnoses, identify therapeutic targets and evaluate treatment efficacy.

DEVELOPMENT OF NEUROIMAGING BIOMARKERS FOR STUDYING AGING AND UNDERLYING MECHANISM IN HUMAN BRAIN

Modern neuroimaging techniques have played important roles in study of human brain aging and diagnosis of neurodegenerative diseases; in particular, Positron Emission Tomography (PET) has been well established to evaluate regional brain glucose and oxygen utilization, neurochemical and neurotransmitter changes, and inflammation in AD and PD brains (Borghammer et al., 2010; Brooks and Pavese, 2011; Niccolini et al., 2014; Varley et al., 2015). For instance, the PET imaging based on radioactive fludeoxyglucose (^{18}FDG) is used to measure the glucose uptake rate that thought to reflect CMR_{Glc}. The ^{18}FDG-PET has been extensively employed to study human brain aging; however, contradictory findings with either negative (Duara et al., 1983, 1984) or positive (Pantano et al., 1984;

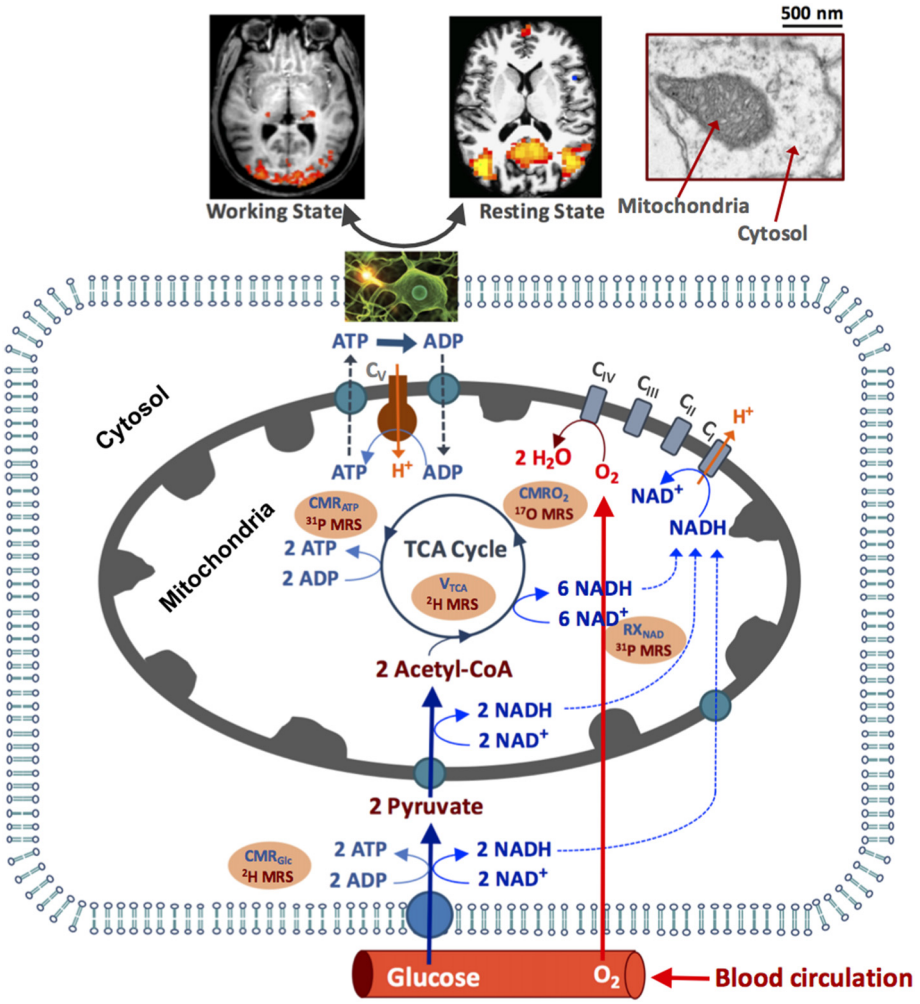

FIGURE 1 | Schematic illustration of major brain hemodynamic and metabolic processes occur in capillary, cytosol and mitochondrial sub-cellular compartments. The feeding arteries supply oxygen and glucose to the cell; glucose is converted to pyruvate, which enters mitochondrial tricarboxylic acid (TCA) cycle and oxidative metabolism pathways. The oxygen utilization is generally coupled with the adenosine triphosphate (ATP) production via the oxidative phosphorylation of adenosine diphosphate (ADP). The ATP is utilized in cytosol to support electrophysiological activities and brain functions at resting and/or working state. The NAD redox reactions are essential in regulating the ATP energy production. The cerebral metabolic rates of glucose (CMR_{Glc}), oxygen ($CMRO_2$) and ATP production (CMR_{ATP}), TCA cycle rate (V_{TAC}) and nicotinamide adenine dinucleotide (NAD) redox ratio (RX_{NAD}) representing the metabolic activities of the brain tissue can be noninvasively measured or imaged using the advanced *in vivo* X-nuclear ^{2}H, ^{17}O and ^{31}P MRS approaches as depicted in the shadowed texts with orange background. C_I-C_V represent five enzyme complexes involving in the cellular respiration chain reactions.

Yamaguchi et al., 1986; Leenders et al., 1990; Marchal et al., 1992; De Santi et al., 1995; Goyal et al., 2017) correlation between actual age and CMR_{Glc} in healthy human have been reported. Note that ^{18}FDG-PET based CMR_{Glc} image reflects the total glucose metabolism through both mitochondrial oxidative phosphorylation and aerobic glycolysis pathways including the conversion of pyruvates (products of glycolysis) into lactates; therefore, it does not directly represent the actual mitochondrial neuroenergetics, which can be determined by $CMRO_2$. Significant $CMRO_2$ reductions in elderly people have been reported, indicating a tight correlation between the mitochondrial energy metabolism and aging (Yamaguchi et al., 1986; Leenders et al., 1990). The $CMRO_2$ decline is consistent with significant decreases in respiratory enzyme (Complexes I–V) activities observed in aging mice brain (Ferrándiz et al., 1994; Navarro and Boveris, 2007), and is in line with a human brain study showing an approximately 30% reduction in both neuronal oxidative glucose metabolism and neurotransmission cycling rates in elderly people (Boumezbeur et al., 2010).

However, there is a lack of sophisticated neuroimaging methods that can quantitatively and noninvasively assess brain mitochondrial enzymatic activities and ATP bioenergetics, even though they play a central role in human aging and neurodegeneration. Most predictive biomarkers offered by neuroimaging are neither sufficiently nor proximal to sub-cellular mechanisms of aging to link mitochondrial and ATP bioenergetic functions. In this article, we will provide

a brief review of several advanced metabolic neuroimaging methods that are based on *in vivo* X-nuclear magnetic resonance (MR) spectroscopic (MRS) imaging (MRSI) at ultra-high magnetic field (UHF) for noninvasive imaging and quantitative assessment of human brain mitochondrial functions and associated bioenergetic biomarkers, which could be highly sensitive to aging without using radioactive tracers. Three *in vivo* X-nuclear MRS methods for imaging cerebral energy metabolisms following specific metabolic pathways are discussed:

1. *In vivo* deuterium-2 (^{2}H) MRSI method for simultaneously measuring CMR_{Glc} and the TCA cycle rate (V_{TCA}),
2. *In vivo* oxygen-17 (^{17}O) MRSI method for quantitatively imaging three physiological parameters: $CMRO_2$, cerebral blood flow (CBF) and oxygen extraction fraction (OEF),
3. *In vivo* phosphorus-31 (^{31}P) MRSI method for simultaneous measurement of cerebral metabolic rates of ATP synthesis via the ATP_{ase} reaction (CMR_{ATP}) and CK reaction (CMR_{CK}), as well as for measuring intracellular NAD^+ and NADH, thus, the NAD redox ratio (RX_{NAD}).

These X-nuclear MRSI methods provide complementary measurements of brain energy metabolisms and ATP bioenergetics following the metabolic roadmap as shown in **Figure 1**.

In vivo carbon-13 (^{13}C) MRS is another X-nuclear MRS method that has been used to study energy metabolism and neurotransmission in animal and human brains. By combining dynamic ^{13}C MRS with ^{13}C-labeled substrates administration and compartmentalized quantification model, the metabolic fluxes of various pathways involving glucose metabolism and neuronal-astrocyte compartmental exchange can be assessed via monitoring the ^{13}C-label incorporation to the major metabolites along these pathways. The strength and limitations of the ^{13}C MRS technique and its applications have been extensively reviewed (e.g., Rothman et al., 2011 #1543; Rodrigues et al., 2013 #1544; Sonnay et al., 2017 #1542), and thus, is covered in this article.

LIMITATIONS OF *IN VIVO* X-NUCLEAR MRSI AND ADVANTAGES OF ULTRA-HIGH FIELD

To apply the *in vivo* X-nuclear MRS or MRSI in biomedical research, we face many challenges, in particular, owing to the very low concentration of detectable metabolites (in the range of few or sub-millimolar (mM)) that is several to tens of thousands of times lower than the tissue water content detected by ^{1}H MRI. Additionally, since the gyromagnetic ratios of the X-nuclei (e.g., ^{2}H, ^{13}C, ^{17}O and ^{31}P) are several times lower than that of ^{1}H, the intrinsic detection sensitivity and signal-to-noise ratio (SNR) of the X-nuclear MRS are further reduced, thus, extensive signal averaging is required to achieve reasonable SNR and spatial resolution. These factors have limited the reliability, applicability and spatiotemporal resolution of the *in vivo* MRSI measurements. To address these limitations, it has been shown that UHF scanners can provide a significant SNR gain and improve spectral and spatial resolutions. The advantages of the UHF for *in vivo* ^{31}P and ^{17}O MRS brain applications are described below.

The ^{31}P nuclide has been studied extensively since the inception of *in vivo* MRS (Shulman et al., 1979; Ackerman et al., 1980; Shoubridge et al., 1982). Besides high energy phosphate compounds (ATP and PCr) and Pi, other phosphorus metabolites such as NAD^+ and NADH that are actively involved in the NAD redox reaction, glycerophosphoethanolamine (GPE), glycerophosphocholine (GPC), phosphoethanolamine (PE) and phosphocholine (PC) which are essential to membrane phospholipid metabolism could also be detected by *in vivo* ^{31}P MRS. The reduced resonance linewidths (in the ppm unit) at higher field will significantly improve the ^{31}P spectral resolution, which makes it possible to resolve adjacent or overlapped phosphate resonances, determine the redox ratio of NAD (Lu et al., 2014b, 2016a; Zhu et al., 2015b), and distinguish intracellular and extracellular Pi *in vivo*. Interestingly, the T_1 values of most phosphorus metabolites decrease at higher fields, presumably the chemical shift anisotropy (CSA) dominates the longitudinal relaxation mechanism at UHF. The shortened T_1 allows more signal averaging per unit sampling time, thus, further improves the SNR and leads to a super linear dependence of the ^{31}P MRS sensitivity on the magnetic field strength (B_0) after considering the B_0 dependences of T_1 and resonance linewidth (Qiao et al., 2006; Lu et al., 2014a).

^{17}O is a stable and NMR detectable isotope of oxygen; it has a very low natural abundance (0.037%) and one-seventh gyromagnetic ratio of the ^{1}H. The ^{17}O isotope with a quantum number of 5/2 obeys the quadrupolar relaxation mechanism, thus, the ^{17}O nuclide in water ($H_2{}^{17}O$) has very short longitudinal (T_1) and transverse (T_2, or apparent T_2: T_2^*) relaxation times (<7 ms) that are insensitive to the B_0 inhomogeneity (Zhu et al., 2001, 2005; Lu et al., 2013). The SNR of the ^{17}O brain water signal has an approximate quadratic field dependence on the static magnetic field strength (i.e., SNR $\propto B_0{}^2$; Zhu et al., 2001; Lu et al., 2013), while the ^{1}H MRI has an approximate linear field dependence (Vaughan et al., 2001). The field dependence of the brain $H_2{}^{17}O$ signal across a wide range of B_0 indicates an over 120 times SNR gain at 16.4T as compared to a 1.5T clinical MRI scanner. Therefore, it is possible to obtain three-dimensional (3D) ^{17}O MRSI of the animal or human brain with adequate SNR and reasonable spatiotemporal resolution at ultrahigh fields. Furthermore, the sensitivity gain at UHF is essential for the development of the *in vivo* ^{17}O MR-based neuroimaging methodology in assessing cerebral oxygen metabolism and perfusion. The UHF advantages are also expected in *in vivo* ^{2}H MRSI applications owing to a similar quadrupolar relaxation mechanism.

SIMULTANEOUS ASSESSMENT OF CMR_{Glc} and V_{TCA} USING *IN VIVO* ^{2}H MRS TECHNIQUE

CMR_{Glc} and V_{TCA} are key parameters presenting the rates of glucose metabolism in brain tissue. Ability to quantify their

values *in vivo* is crucial for assessing the metabolic and energetic states of the brain. As shown in **Figure 1**, the stoichiometric ratio of the CMR_{Glc} and V_{TCA} in normal brain is approximately two to one since one glucose can produce two pyruvates in cytosol before entering the mitochondrial TCA cycle; such coupling relationship can change under pathological condition, e.g., in brain tumor or stroke. Even though it is challenging, quantitative and simultaneous imaging of both CMR_{Glc} and V_{TCA} is desired for studying the complex glucose metabolic pathways and their contributions to the ATP production under normal and diseased states. Recently, we have developed an *in vivo* ^{2}H MRS technique for simultaneous CMR_{Glc} and V_{TCA} measurement; this technique has been validated at 16.4T using a preclinical rat model (Lu et al., 2017).

^{2}H nuclide is a stable isotope of hydrogen with a quantum number of 1 and has an extremely low natural abundance (0.0156%). Like ^{17}O nuclide, molecules containing ^{2}H obey quadrupolar relaxation mechanism and have short T_1 and T_2 values that enables rapid signal averaging for gaining the SNR. Thus, the *in vivo* ^{2}H MRS or MRSI becomes attractive at UHF when combining with ^{2}H-isotope (deuterium) labeled glucose infusion (Mateescu et al., 2011; Lu et al., 2017). After infusion, several deuterium labeled compounds, including the glycolysis and TCA cycle intermediates of the brain tissue, e.g., glutamate/glutamine (Glx), lactate (Lac) and water, can be detected using the UHF ^{2}H MRS with excellent sensitivity and temporal resolution and identified based on their well-resolved ^{2}H resonances and chemical shifts. The robust ^{2}H MRS signal detection, spectral analysis and kinetic modeling eventually allow for quantification of CMR_{Glc} and V_{TCA} in live brains.

Figure 2A displays the ^{2}H-isotope labeling scheme, labeled metabolites and associated metabolic pathways following an intravenous D-Glucose-6,6-d_2 (d66) infusion (Mateescu et al., 2011; Lu et al., 2017), where d66 glucose and non-labeled glucose are transported together into the brain and metabolized via glycolysis and oxidative phosphorylation. Along the metabolic pathways, the deuterium label on d66 can incorporate into the Lac, Glx and water pools, which can then be monitored through dynamic ^{2}H MRS acquisitions. Excellent spectral quality and spectral fittings can be obtained not only from d66 phantom solution (with water resonance set at 4.8 ppm as a chemical shift reference) but also from living rat brain; for instance, well-resolved deuterated resonances of glucose (3.8 ppm), Glx (2.4 ppm) and lactate (1.4 ppm) were detected following a brief (2 min) d66 infusion (**Figure 2B**). Their dynamic signal changes (15 s temporal resolution) were used to determine the CMR_{Glc} and V_{TCA} values based on a simplified kinetic model (Lu et al., 2017). The *in vivo* ^{2}H MRS approach has been applied to rat brains under isoflurane anesthesia and morphine analgesic condition; significant reduction of CMR_{Glc} and V_{TCA} in rat brains under 2% isoflurane (CMR_{Glc} = 0.28 ± 0.13 and V_{TCA} = 0.6 ± 0.2 μmol/g/min) as compared to that of morphine (CMR_{Glc} = 0.46 ± 0.06 and V_{TCA} = 0.96 ± 0.4 μmol/g/min) were found (Lu et al., 2017), suggesting that the *in vivo* ^{2}H MRS technique is highly sensitive in detecting the cerebral metabolic rate changes.

Compared with the *in vivo* ^{13}C MRS (Gruetter et al., 2003), several merits of the *in vivo* ^{2}H MRS technology are worth mentioning: (i) the short T_1 relaxation time of the quadrupolar ^{2}H nuclide (e.g., ∼50 ms for d66 in rat brain at 16.4T; Lu et al., 2017) enables rapid sampling to significantly increase the SNR for *in vivo* ^{2}H MRS or MRSI application (see an example in **Figure 2B**); (ii) the chemical shift assignments (in ppm) and spectral patterns of the deuterated metabolites are almost identical to that of *in vivo* ^{1}H MRS, while the chemical shift range (in Hz) of the ^{2}H spectrum is ∼7 times narrower than that of ^{1}H MRS due to a much lower ^{2}H gyromagnetic ratio (6.5 MHz/T for ^{2}H vs. 42.6 MHz/T for ^{1}H), thus, the chemical shift displacement artifacts should be significantly reduced for ^{2}H MRS localization, especially at UHF (Chen and Zhu, 2005; Lu et al., 2017); on the other hand, it is challenging to study the neurotransmission cycling between neuron and glia cells using the ^{2}H MRS method due to the inability of resolving ^{2}H-labeled glutamate from glutamine (Sibson et al., 2001; Hyder et al., 2006); (iii) in an *in vivo* ^{2}H MRS spectrum, the natural abundant water signal of the brain tissue can serve as an internal reference for quantifying cerebral metabolites labeled with deuterium, which makes metabolites quantification easier and more reliable; and (iv) there is no background contamination in the ^{2}H spectrum of living brain because no natural abundance metabolite signal other than water is detectable *in vivo*, therefore, technique commonly applied in ^{13}C and ^{1}H MRS to suppress intense water or lipid signal is no longer needed.

The *in vivo* ^{2}H MRS approach could be highly valuable for studying the decoupled relationship between glycolysis and oxidative metabolism and image the Warburg effect in brain tumor. This can be achieved through directly measuring the metabolic rates of CMR_{Glc} and V_{TCA} using the ^{2}H MRSI approach or by simply mapping the Glx/Lac ratio (ideally measured when Glx and Lac signals reaching a plateau after the introduction of d66), which could provide a sensitive index of the Warburg effect in brain tumor (Lu et al., 2016b). To establish a completely noninvasive metabolic imaging based on the *in vivo* ^{2}H MRSI measurement, the intravenous infusion of the d66 tracer can be replaced by an oral delivery of d66. The feasibility of introducing d66 via oral intake for CMR_{Glc} and V_{TCA} measurement has been recently demonstrated (Lu et al., 2018), which paves the way for translational application.

NON-INVASIVE IMAGING OF $CMRO_2$, CBF AND OEF USING *IN VIVO* ^{17}O MR TECHNIQUE

The motivation of developing *in vivo* ^{17}O MR imaging techniques is to measure $CMRO_2$ via monitoring the dynamic change of the $H_2{}^{17}O$ water that is metabolized from ^{17}O-labeled O_2 gas (Mateescu et al., 1989; Pekar et al., 1991; Fiat and Kang, 1992, 1993; Reddy et al., 1996; Arai et al., 1998; Ronen et al., 1998; Zhu et al., 2002; Zhang et al., 2004; Atkinson and Thulborn, 2010; Kurzhunov et al., 2017; Niesporek et al., 2018). Generally, *in vivo* ^{17}O-MR imaging method shares a similar principle as the well-established ^{15}O-PET technique (Lenzi et al., 1981;

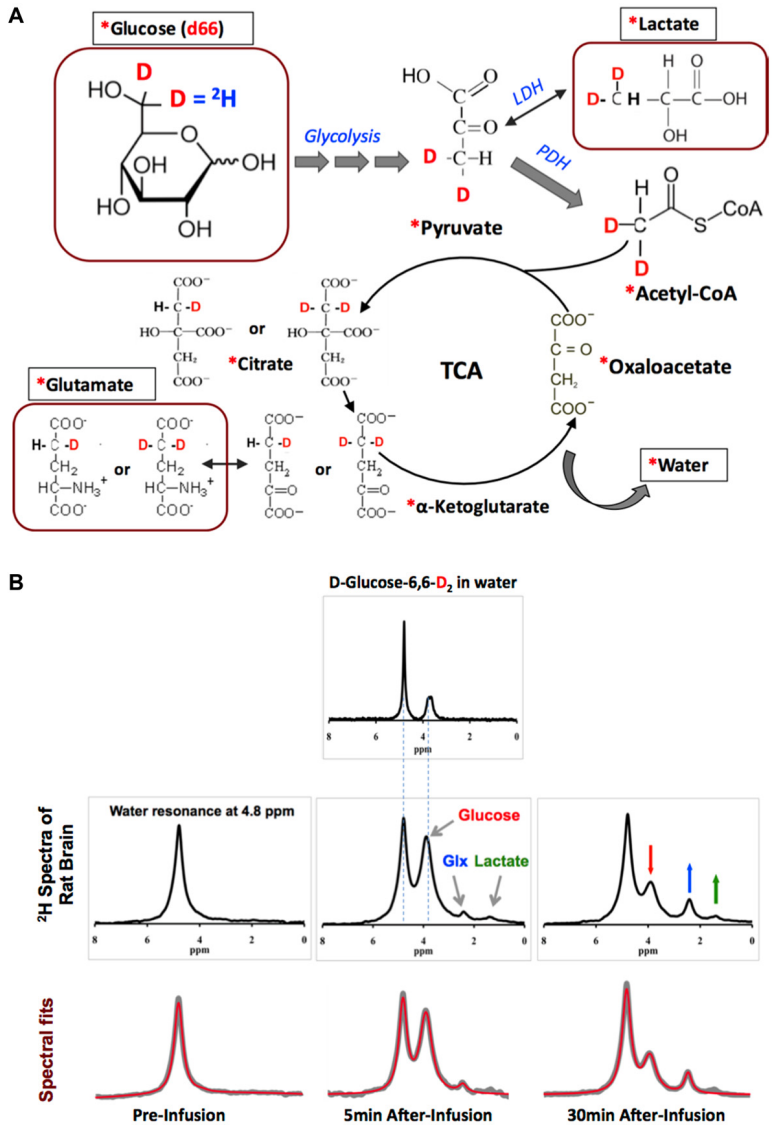

FIGURE 2 | (A) The ^{2}H-labeling scheme following the metabolic pathways of isotope-labeled glucose D-Glucose-6,6-d_2 (d66). The ^{2}H-labeled glucose first incorporates into pyruvate pool through glycolysis to form [3,3-d_2] pyruvate, some of which can be converted to [3,3-d_2] lactate by lactate dehydrogenase (LDH). [3,3-d_2] Pyruvate can also be transported into the mitochondria to form [2,2-d_2] Acetyl-CoA catalyzed by pyruvate dehydrogenase (PDH). After entering the TCA cycle, intermediates (4-d) or [4,4-d_2] citrate and (4-d) or [4,4-d_2] α-ketoglutarate could exchange with glutamate to generate (4-d) or [4,4-d_2] glutamate. In this process, the ^{2}H-labels may exchange with the proton(s) in water molecule to form deuterated water and depart from the cycle. "*": Pools labeled with ^{2}H; square boxes: highlighting the metabolites detectable by *in vivo* ^{2}H MRS. **(B)** Representative original (upper rows black traces and bottom row gray traces) and fitted (red traces in bottom row) ^{2}H spectra obtained from deuterated glucose (d66) phantom solution (top panel), and in rat brain pre- (left column) and 5 or 30 min post-deuterated glucose (d66) infusion. ^{2}H resonance assignments: water at 4.8 ppm (use as a chemical shift reference); glucose at 3.8 ppm; mixed glutamate and glutamine (Glx) at 2.4 ppm; and lactate at 1.4 ppm. Figure adapted from Lu et al. (2017).

Mintun et al., 1984) for imaging $CMRO_2$. Both modalities apply isotope-labeled oxygen gas inhalation in the measurement: $^{17}O_2$ for ^{17}O-MR and $^{15}O_2$ for ^{15}O-PET. After the inhalation, the isotope-labeled O_2 molecules bind to hemoglobin during the gas exchange in the lung and are subsequently delivered to the brain cells through blood circulation, perfusion and diffusion, and reduced by the cytochrome oxidase in the mitochondria to form the isotope-labeled water. One labeled oxygen molecule produces two labeled water molecules in the mitochondria, which can be washed out from the brain cells, enter the venous system and back to the heart via blood circulation.

Despite the common principle, there are fundamental differences between the ^{17}O-MR and ^{15}O-PET techniques in imaging $CMRO_2$. ^{15}O-PET cannot distinguish the radioactive signals attributed from the metabolic substrate ($^{15}O_2$) and the metabolic product ($H_2{}^{15}O$). Therefore, a standard PET-based $CMRO_2$ imaging method requires a complicate $CMRO_2$ quantification model plus multiple measurement procedures

with: (i) inhalation of $^{15}O_2$ gas; (ii) injection of $H_2{}^{15}O$ tracer; and (iii) inhalation of $C^{15}O$ gas (Mintun et al., 1984), which substantially increase the total scanning time, radioactive dose and the measurement cost. The *in vivo* ^{17}O MR imaging method, on the other hand, only detects the metabolically generated and isotope-labeled $H_2{}^{17}O$. $^{17}O_2$ molecules, either freely dissolved or bound to hemoglobin are "invisible" to the *in vivo* ^{17}O detection (**Figure 3**) owing to the extremely broad ^{17}O resonance linewidth (Zhu et al., 2005; Zhu and Chen, 2011). This feature greatly simplifies the ^{17}O-MR based $CMRO_2$ imaging measurement that uses a non-radioactive and stable isotope, and thus, is more safer for human application (Zhang et al., 2004; Zhu et al., 2005; Atkinson and Thulborn, 2010).

The dynamics of the ^{17}O MR signal from the brain tissue $H_2{}^{17}O$ measured during and after an $^{17}O_2$ inhalation reflects an interplay of three physiological processes: (i) oxygen consumption to produce labeled $H_2{}^{17}O$ in the mitochondria, (ii) washout of labeled $H_2{}^{17}O$ from the brain cells via blood circulation, and (iii) "recirculation" of labeled $H_2{}^{17}O$ generated in the body re-entering the brain. The mass balance equation accounted the contributions from all three processes can be used for $CMRO_2$ quantification (Pekar et al., 1991; Zhu et al., 2002, 2005; Zhang et al., 2004; Atkinson and Thulborn, 2010):

$$\frac{dC_b(t)}{dt} = 2 \cdot \alpha(t)\, CMRO_2 + CBF \cdot \left[C_a(t) - \frac{C_b(t)}{\lambda} \right] \quad (1)$$

where $C_a(t)$, and $C_b(t)$ are the time-dependent and ^{17}O-isotope labeled $H_2{}^{17}O$ concentration in the arterial blood and brain tissue, respectively; $\alpha(t)$ is the ^{17}O enrichment fraction of the blood-contained $^{17}O_2$; λ is the brain/blood partition coefficient; the factor of 2 in Equation 1 accounts for the production of two $H_2{}^{17}O$ molecules from one $^{17}O_2$ molecule (Zhu et al., 2002; Zhang et al., 2004).

As demonstrated in **Figure 3**, there are three distinct phases in the brain $H_2{}^{17}O$ time course covering the baseline, inhalation and post-inhalation periods (Zhu et al., 2002). The signals in the first phase representing the natural abundance $H_2{}^{17}O$ in the brain tissue can serve as an internal reference for quantifying the brain $H_2{}^{17}O$ concentration and its change during the second and third phases. Equation 1 can be employed to calculate the $CMRO_2$ and CBF values, and estimate OEF (detailed quantification modeling and simplified approaches can be found in the literature (Zhu et al., 2002, 2013a,b).

One attractive feature of the ^{17}O-MR based $CMRO_2$ imaging approach is it enables repeated $CMRO_2$ measurements since the metabolized $H_2{}^{17}O$ signal in the brain can reach a new steady-state within a short time (e.g., <10 min in rodents, see **Figure 3**) at the end of the $^{17}O_2$ inhalation, so subsequent $CMRO_2$ measurements can be performed in the same subject within the same imaging session (Zhu et al., 2007). This capability is important for studying $CMRO_2$, CBF and OEF and their changes due to physiopathological perturbations where multiple measurements under different conditions are required.

For example, **Figure 4A** illustrates a functional study of blood oxygenation level dependent (BOLD) contrast and $CMRO_2$ changes in cat brain during visual stimulation (Zhu et al., 2009). Two 3D ^{17}O $CMRO_2$ imaging measurements, with and without visual stimulation, were performed on each animal. A significant increase in $CMRO_2$ (~30%) was detected in the activated visual cortical regions (**Figures 4A,B**); and interestingly, a strong inverse relation between the baseline $CMRO_2$ level and stimuli-induced $CMRO_2$ relative change across different subjects (**Figure 4C**) was observed (Zhu et al., 2009). **Figure 4D** demonstrates a preclinical application of the quantitative ^{17}O-MR imaging methodology for simultaneous and completely noninvasive mapping of $CMRO_2$, CBF and OEF in mouse brain using a brief $^{17}O_2$ inhalation (2–3 min), showing impaired $CMRO_2$ and CBF and elevated OEF in the ischemic brain region as compared to the intact brain tissue in the contralateral hemisphere (Zhu et al., 2013a).

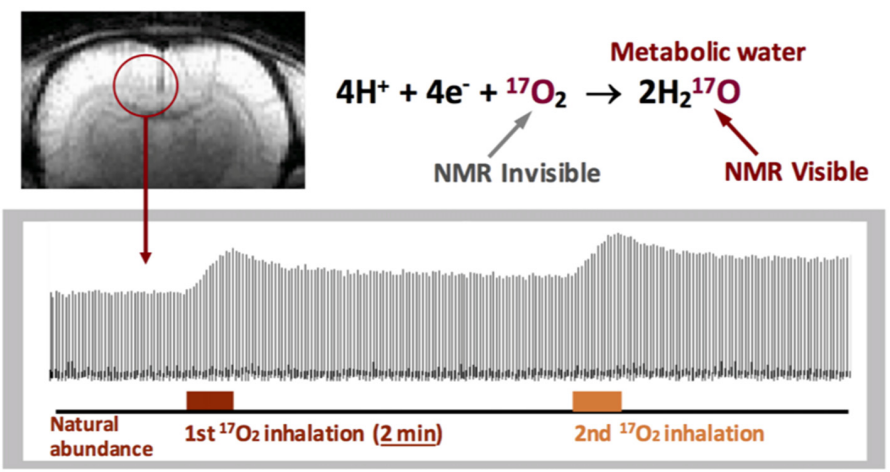

FIGURE 3 | Stack plots of rat brain tissue $H_2{}^{17}O$ spectra obtained from a single voxel selected from the 3D ^{17}O MRSI datasets with two consecutive $^{17}O_2$ inhalations (~2 min each) for repeated $CMRO_2$ and cerebral blood flow (CBF) imaging measurements. $^{17}O_2$ in either blood or brain tissue is NMR invisible. Figure adapted from Zhu et al. (2007).

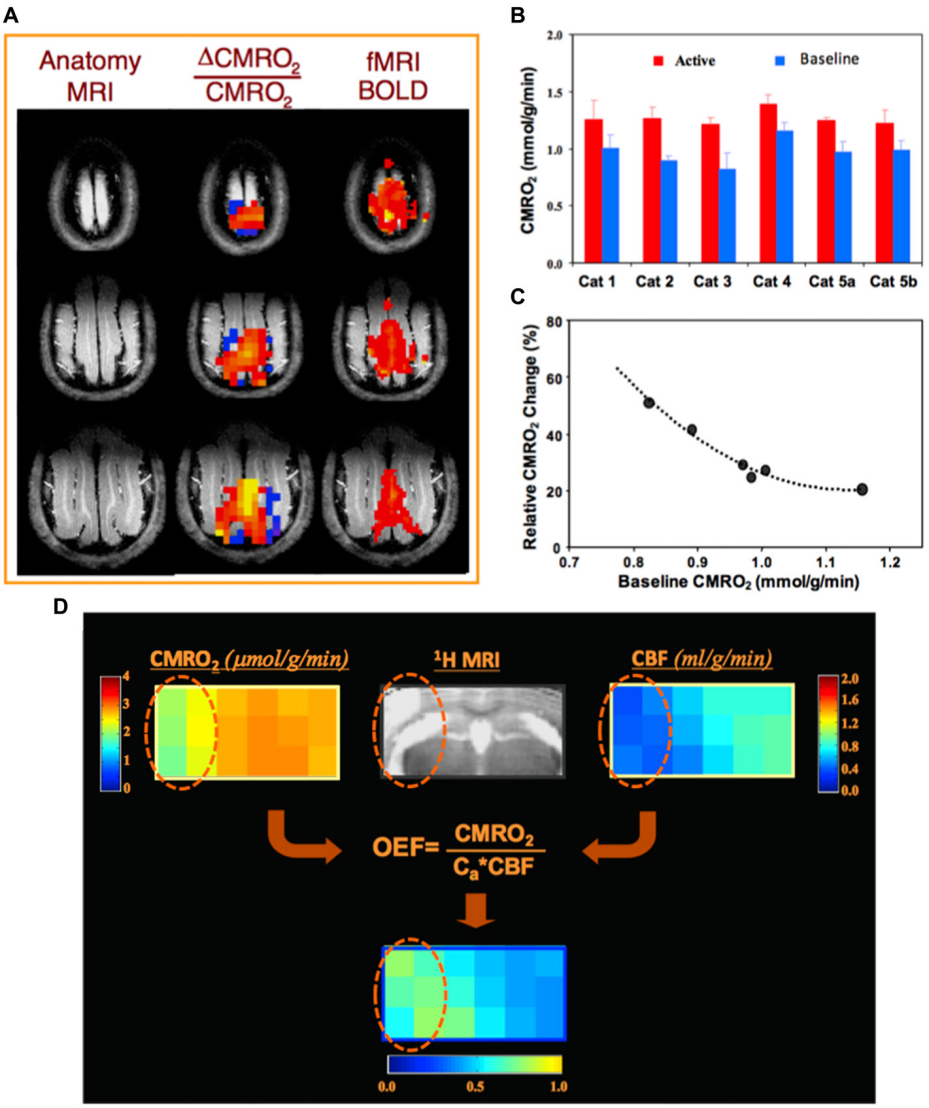

FIGURE 4 | (A) Anatomic brain images (left), fMRI blood oxygenation level dependent (BOLD) maps (right) and corresponding 3D functional $CMRO_2$ activation maps (middle) obtained from three representative image slices in a cat visual cortex, showing a significant $CMRO_2$ increase during visual stimulation. **(B)** Individual $CMRO_2$ values measured from the activated cat visual cortex region during visual stimulation as well as at control condition (baseline). Two functional studies conducted at different days in Cat 5, showing excellent $CMRO_2$ imaging reproducibility. **(C)** A strong correlation of baseline $CMRO_2$ level and activated $CMRO_2$ change among individual animals. Figure adapted from Zhu et al. (2009). **(D)** *In vivo* ^{17}O MRS imaging from a representative image slice in a mouse with middle cerebral artery occlusion (MCAO) preparation, showing significant reductions of $CMRO_2$ and CBF, and an elevated oxygen extraction fraction (OEF) in the ischemic brain region (cycled) affected by MCAO as compared to the intact tissue in the contralateral hemisphere. Figure adapted from Zhu et al. (2013a) with permission of Elsevier Inc.

For human brain application, due to the large body size, slow blood circulation and exchange of ^{17}O labeled and non-labeled oxygen gas in human lung, it is more challenging to reliably quantify $CMRO_2$, and a more sophisticated $CMRO_2$ quantification model is required (Atkinson and Thulborn, 2010; Zhu et al., 2014). Recently, we have demonstrated the feasibility for noninvasively imaging all three parameters of $CMRO_2$, CBF and OEF using a brief (2–3 min) $^{17}O_2$ inhalation in human visual cortex under resting condition and their changes in response to visual stimulation (Zhu et al., 2014).

STUDYING CEREBRAL ATP ENERGY METABOLISM AND NAD REDOX USING *IN VIVO* ^{31}P MRS TECHNIQUE

In vivo ^{31}P MRS is a powerful tool for studying cerebral phosphorus metabolism and neuroenergetics without the need for any isotopically labeled substrate. It not only detects various phosphorus metabolites, but also determines intracellular pH and free Mg^{2+} concentration of the brain tissue (Ackerman et al., 1980; Hetherington et al., 2002; Lei et al., 2003b; Du et al.,

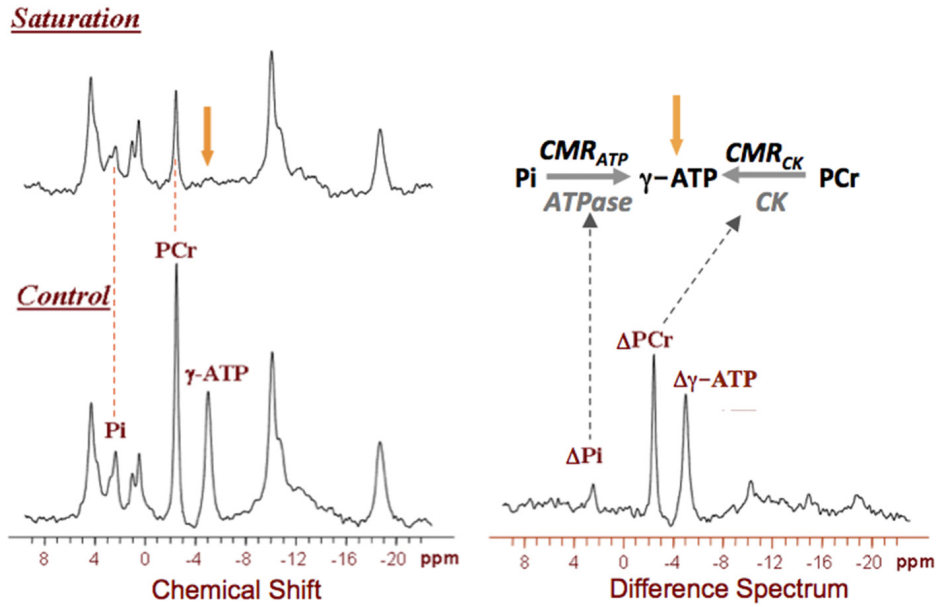

FIGURE 5 | *In vivo* ^{31}P spectra obtained from a representative healthy human brain in the absence (control) and presence of γ-ATP resonance saturation at 7T, and their difference spectrum. The signal reductions in the Pi and Phosphocreatine (PCr) resonances can be used to calculate the values of CMR_{ATP} and CMR_{CK}, respectively. Figure adapted from Lei et al. (2003a).

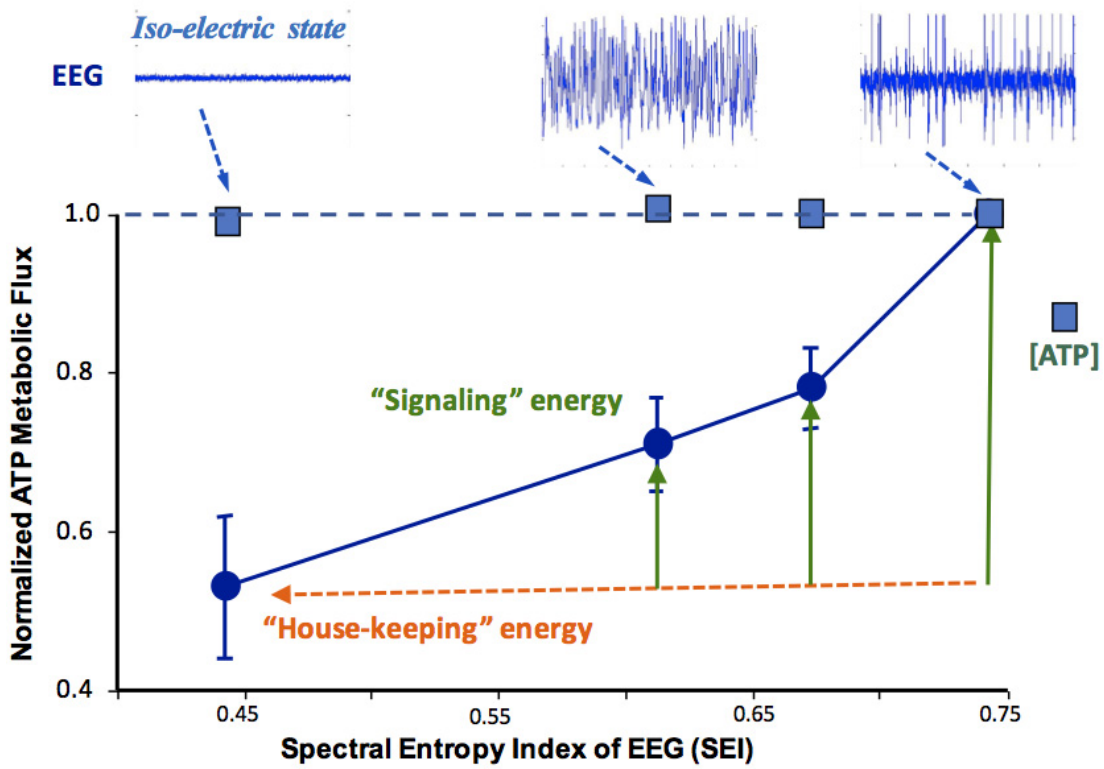

FIGURE 6 | Relationship of the rat brain electroencephalogram (EEG) activity level (top tracers) and normalized CMR_{ATP} or cerebral ATP concentration determined under different brain states. The EEG signal was quantified by the spectral entropy index (SEI). The CMR_{ATP} value correlates strongly with SEI, while intracellular ATP concentration remains constant even at the iso-electric state. Figure adapted from Du et al. (2008).

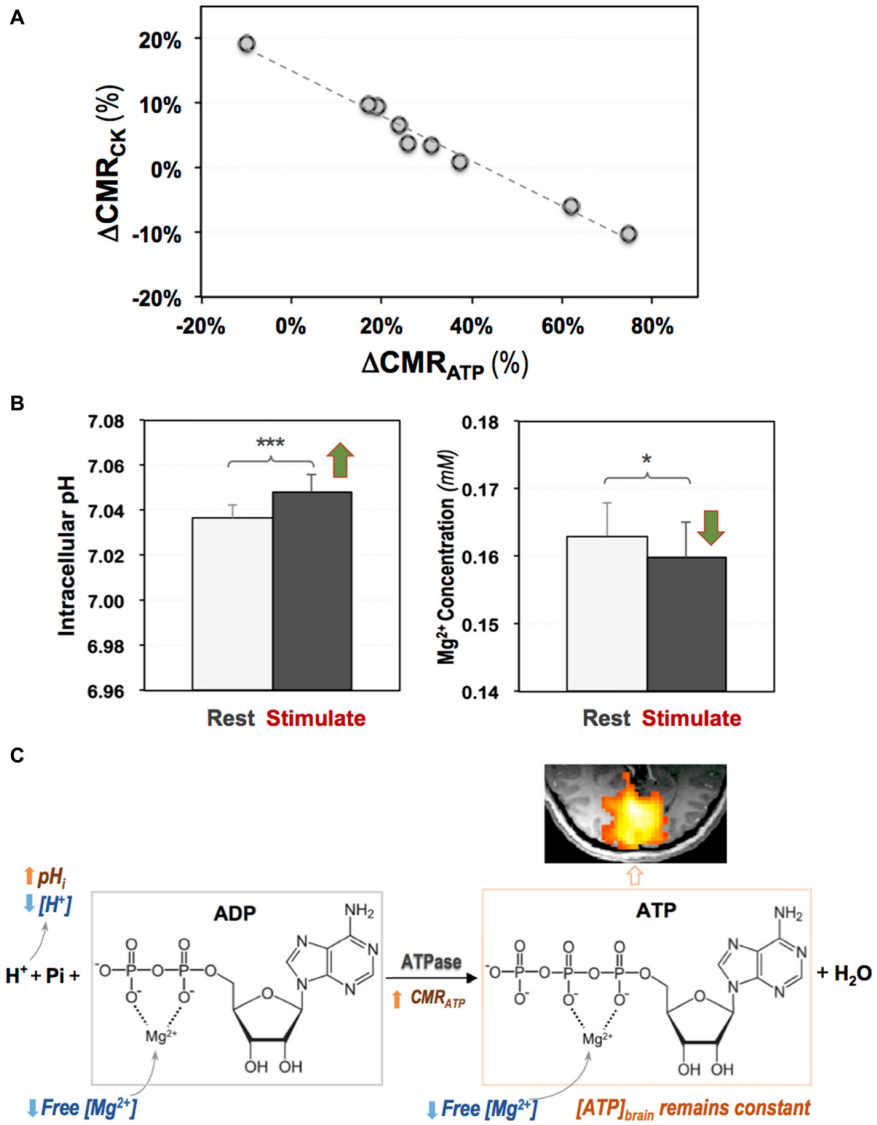

FIGURE 7 | (A) A strong and negative correlation between the stimulus-evoked CMR_{CK} and CMR_{ATP} changes among individual subjects; and **(B)** increased intracellular pH and decreased intracellular free Mg^{2+} level in human visual cortex during visual stimulation. **(C)** Schematic illustration of complex and coherent changes in ATPase activity, ATP production rate (CMR_{ATP}), intracellular pH and free (Mg^{2+}) in response to brain stimulation (Zhu et al., 2018). Two-tailed paired *t*-test indicating significant differences detected comparing the two conditions with $^{*}p < 0.05$ and $^{***}p < 0.001$.

2007, 2008; Zhu et al., 2012). Furthermore, when it combines with the magnetization transfer (MT) preparation (^{31}P MRS-MT), the enzyme activities and metabolic fluxes via the F_1F_0-ATPase and CK reactions can be measured and quantified (Frosén and Hoffman, 1963; Shoubridge et al., 1982; Uğurbil, 1985; Lei et al., 2003a; Du et al., 2007; Ren et al., 2017). Therefore, the *in vivo* ^{31}P MRS-MT technique can be used to noninvasively study abnormal mitochondrial function associated with energetic impairment in neurodegenerative diseases such as AD (Schägger and Ohm, 1995). **Figure 5** displays a typical ^{31}P MRS-MT dataset obtained in human brain at 7T. The signal reductions of the PCr and Pi resonances in the presence of γ-ATP saturation as compared to that of control can be used to calculate the "forward" metabolic fluxes for the CK reaction (i.e., PCr→ATP) and ATPase reaction (i.e., Pi→ATP), i.e., CMR_{CK} and CMR_{ATP}, respectively (Lei et al., 2003a; Du et al., 2007).

As shown in **Figure 6**, the *in vivo* ^{31}P MRS-MT method can be used to investigate the relation between the neuronal activity level and the ATP production rates at different brain states (Du et al., 2008). In this study, a strong positive correlation between the spontaneous brain electroencephalogram (EEG) activity and CMR_{ATP} was reported (Du et al., 2008); it was also found that when all electrophysiological signals are stopped (i.e., in an isoelectric state), the brain still consumes a significant portion of ATP energy for "house-keeping"

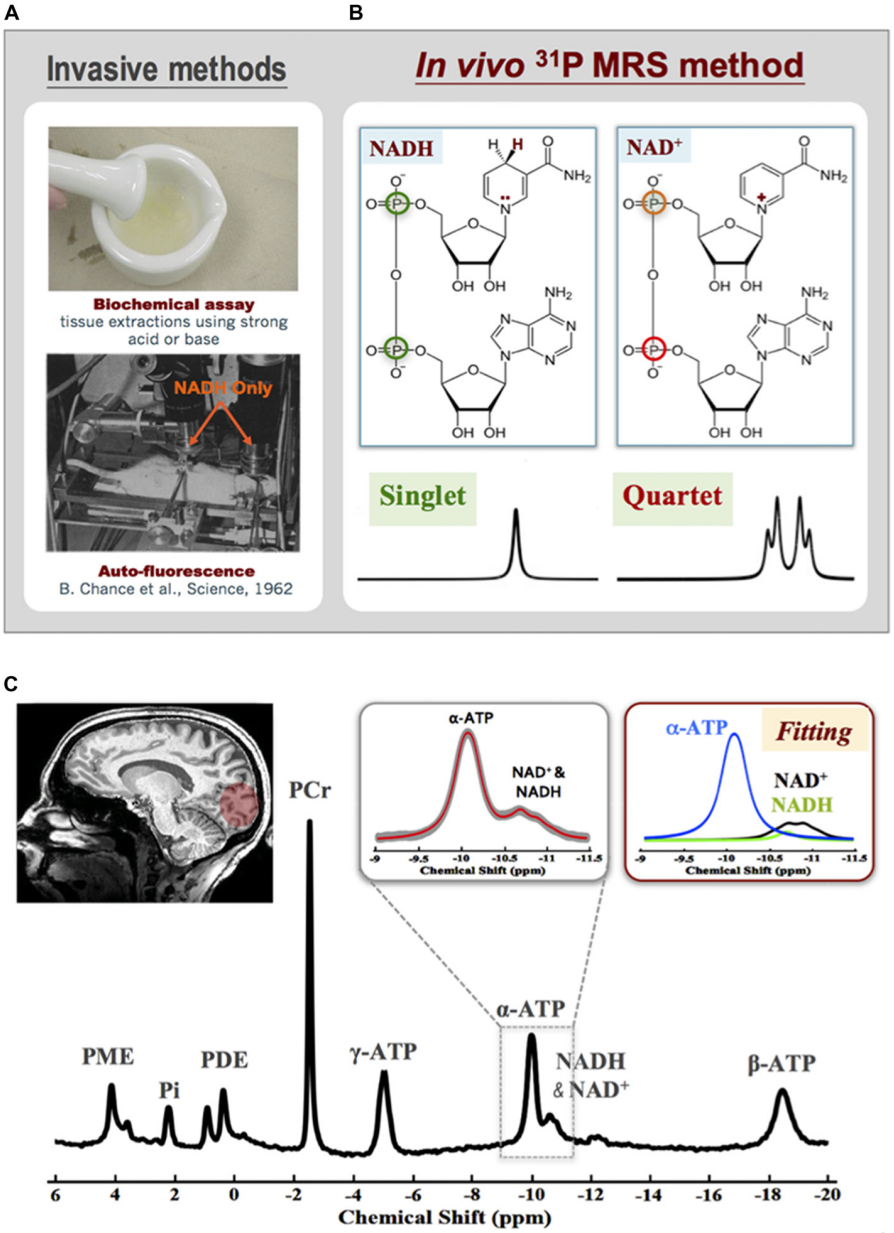

FIGURE 8 | (A) Two invasive methods are available for assessing intracellular NAD contents based on biochemical assay (top) or auto-fluorescence technique. **(B)** Molecular structures of NAD^+ and NADH and their distinct ^{31}P spectral patterns (singlet for NADH and quartet for NAD^+). **(C)** A representative ^{31}P spectrum obtained from the occipital lobe of a healthy subject at 7T. The expanded spectra in the inserts display a chemical shift range of −9.0 to −11.5 ppm with original ^{31}P signal (gray trace) and model fitted spectrum (red trace) of α-ATP and NAD. The individual fitting components of γ-ATP (blue), NAD^+ (black) and NADH (green) are also showed in the top-right panel. Figure adapted from Zhu et al. (2015b).

and maintaining the cellular integrity; and the brain ATP concentration remains constant while CMR_{ATP} could vary ∼50% over a wide range of neuronal activity levels (see **Figure 6**). These findings suggest that under physiological conditions, the cerebral energy metabolism is effectively regulated to maintain the intracellular ATP homeostasis; and the metabolic rate of CMR_{ATP} should be a better biomarker for assessing energetic state of healthy brains (Du et al., 2008).

With improved sensitivity and spectral resolution at ultrahigh field of 7T and advancement in developing UHF radiofrequency (RF) coils, *in vivo* ^{31}P MRS-MT approach can be combined with 3D chemical shift imaging (CSI) to map the ATP metabolic rates in human brain with whole-head coverage. This makes it possible to differentiate CMR_{ATP} and CMR_{CK} between the human brain gray matter (GM) and white matter (WM), which led to the finding of three times higher CMR_{ATP} and CMR_{CK} in GM than WM. Also, it has been found that on average, a single neuron

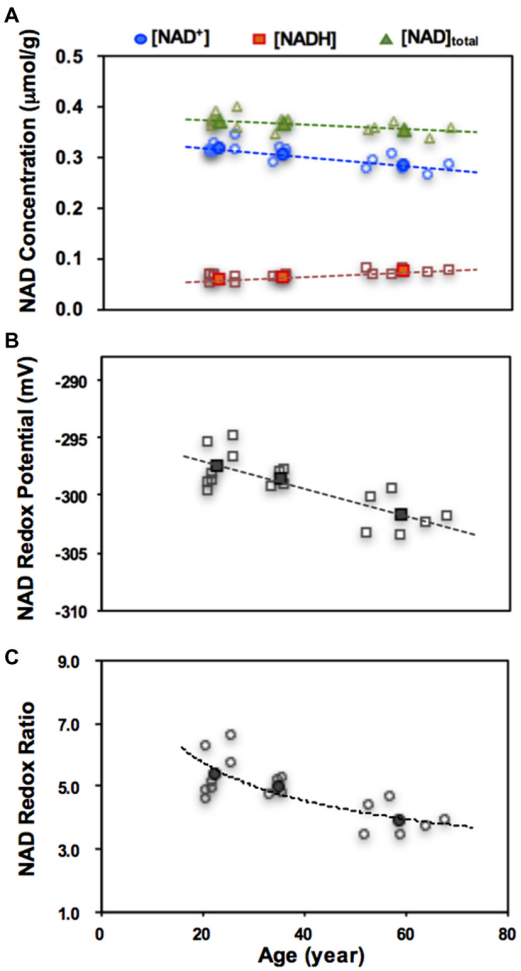

FIGURE 9 | Age dependences of intracellular NAD^+, NADH, total NAD concentrations **(A)**, the NAD redox potential **(B)** or redox ratio **(C)** observed in healthy human brains. The open symbols represent data of individual subjects and the filled symbols are the average data from three age groups of young (21–26 year, $n = 7$), middle (33–36 year, $n = 4$) and old (59–68 year, $n = 6$) subjects. Figure adapted from Zhu et al. (2015b).

consumes ∼4.7 billion ATP molecules per second in human cortex at resting condition based on the direct CMR_{ATP} imaging measurement (Zhu et al., 2012).

Given the high ATP expenditure in a resting human brain, how a brain at working-state fulfills its energetic requirement is an important question for understanding the fundamental role of cerebral energetics in brain function and health. By applying the 3D ^{31}P CSI-MT imaging technique in human visual cortex at 7T, the regional CMR_{ATP} and CMR_{CK} at rest and during visual stimulation were directly measured; and a significant stimulus-induced and highly correlated neuroenergetic changes was detected, indicating that the ATPase and CK reactions play distinctive and complementary roles in supporting evoked neuronal activity and maintaining the intracellular ATP homeostasis (Zhu et al., 2018). **Figure 7** summarizes the results of this study showing a strong and negative correlation between the task-evoked CMR_{ATP} and CMR_{CK} changes in the activated human visual cortex among individual subjects (**Figure 7A**), and a significant increase in the intracellular pH accompanied by a reduction in the intracellular free $[Mg^{2+}]$ during the visual stimulation (**Figure 7B**). The findings of this original study provide interesting new insights into the mechanism of brain ATP energy metabolism and regulation in supporting evoked neuronal activity (**Figure 7C**), and demonstrate that the *in vivo* ^{31}P-MT imaging technique is a sensitive and highly valuable neuroimaging tool for quantitatively studying energy metabolism in human brain.

Brain energy metabolism and regulation are controlled by the metabolic coenzyme NAD and its redox state presented by the parameter of RX_{NAD} (= $[NAD^+]$/[NADH]). Extensive biological and cellular studies indicate that NAD^+ also functions as a co-substrate for several important enzymes including Sirtuins, poly-ADP-ribose polymerases (PARPs) and CD38/157 that play critical roles in cellular signaling, cell death, aging and longevity. Intracellular NAD^+ depletion has emerged as an indicator of aging and neurodegeneration, and thus, it is considered as a new therapeutic target for aging-related disorders and neurodegenerative diseases (Ying, 2007; Mouchiroud et al., 2013; Imai and Guarente, 2014; Verdin, 2015; Guarente, 2016; Mills et al., 2016; Schultz and Sinclair, 2016; Fang et al., 2017).

Despite the crucial roles of NAD in cellular energy metabolism and signaling, determining intracellular NAD contents and redox state is difficult, especially in live brains. Only two invasive methods are available: one is the biochemical assay (Zhang et al., 2006; Yang et al., 2007; Xie et al., 2009) and the other relies on the auto-fluorescence signal of the NADH but not NAD^+ (Chance et al., 1962; see **Figure 8A**). Few years ago, an *in vivo* ^{31}P MRS-based NAD assay was developed in our laboratory that enables noninvasive assessment of NAD^+ and NADH contents and RX_{NAD} in animal and human brains (Lu et al., 2014b, 2016a; Zhu et al., 2015b). This new method utilizes a theoretical NMR spectral model to describe the ^{31}P resonances of NAD^+ and NADH and their spectral patterns at a given magnetic field strength. As shown in **Figure 8B**, the molecular structure of NAD^+ only differs from NADH by one H^+ and two electrons. This subtle structural difference makes the shielding environment of the phosphorus spins in the NAD^+ molecule (two different ^{31}P spins) substantially different from that of NADH (two identical ^{31}P spins). Based on the NMR theory, the second-order coupling effect applies to the two-spin system of NAD^+, leading to a well-defined quartet of resonances with the signal intensity ratios and chemical shifts varying with the field strength; conversely, the NADH displays a single resonance with doubled intensity. The spectral patterns of NAD^+ quartet and NADH singlet, therefore, can be precisely predicted at any given field strength using a quantification model that describes all ^{31}P signals of NAD^+, NADH and α-ATP. After least-square fitting of the *in vivo* ^{31}P spectrum, the values of $[NAD^+]$, [NADH] and RX_{NAD} can be calculated using the α-ATP signal as an internal concentration reference (Lu et al., 2014b). The newly developed *in vivo* NAD assay has been applied to the healthy human at 7T. Excellent SNR and spectral quality as shown in **Figure 8C** ensures the reliable fitting of NAD^+, NADH and α-ATP resonances and the quantification of $[NAD^+]$ (≈0.30 ± 0.02 mM), [NADH]

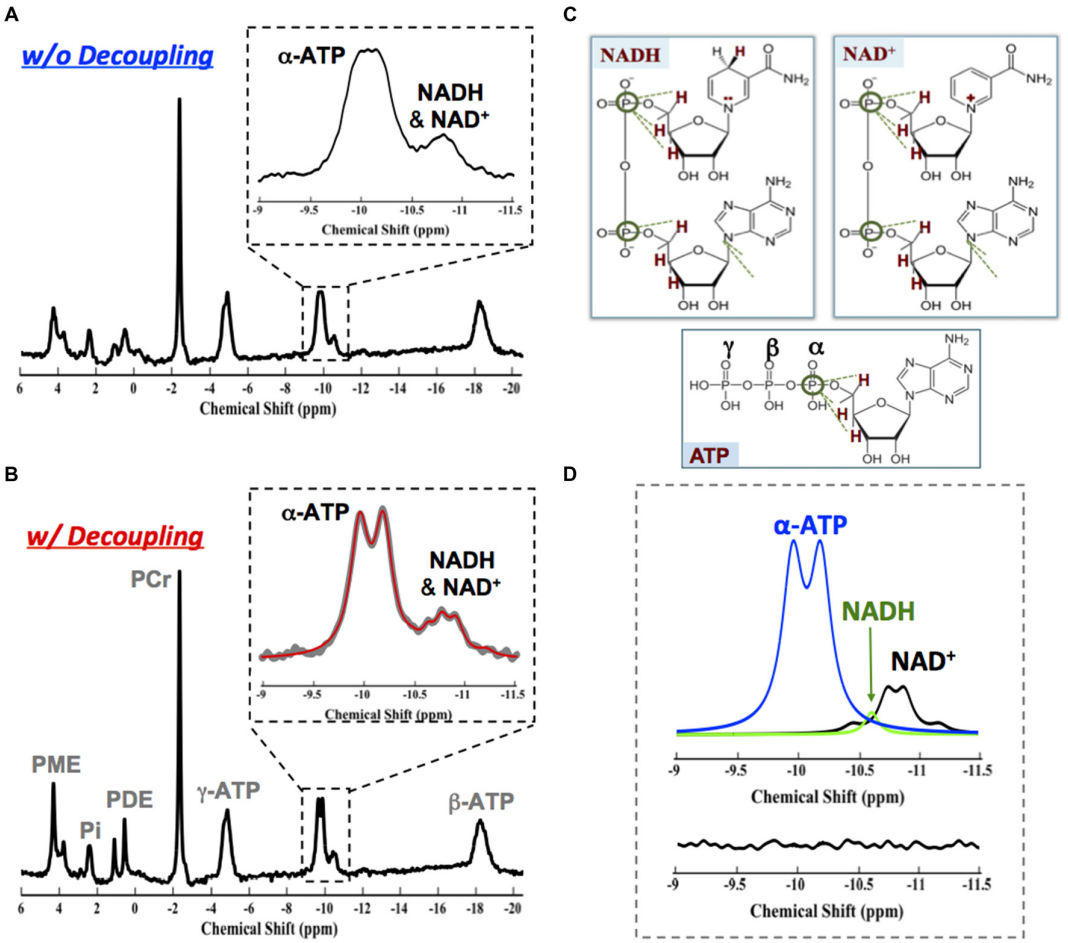

FIGURE 10 | *In vivo* ^{31}P brain spectrum collected in the absence **(A)** and presence **(B)** of ^{1}H decoupling on the water resonance from a representative healthy subject at 4T. The ^{1}H decoupling significantly reduces the linewidth of γ-ATP, NAD^+ and NADH resonances owing to the close proximity between their phosphorus spins to the protons as shown in **(C)**. **(D)** Fitting results showing individual components of γ-ATP (blue), NAD^+ (black) and NADH (green) signals and a small residue. Figure adapted from Lu et al. (2016a).

(≈0.06 ± 0.01 mM) and RX_{NAD} (= 4.8 ± 0.9) in the healthy human brain (Zhu et al., 2015b).

A growing number of evidence suggests a close link between the abnormal brain NAD^+ and amyloid beta-peptide in AD (Wu et al., 2014), and therapies that aim to restore intracellular NAD^+ level have shown promise for repairing the DNA damage or protecting against age-related cellular damage (Braidy et al., 2008, 2011). The ^{31}P MRS-based *in vivo* NAD assay provides an ideal tool to monitor the NAD changes in the human brain. **Figure 9** shows an application of the NAD assay in healthy subjects, which detected strong age-dependent changes in $[NAD^+]$, [NADH], $[NAD]_{total}$ (=$[NAD^+]$+[NADH]) and RX_{NAD} (Zhu et al., 2015b). A decrease in the NAD^+/NADH redox ratio in normal human brain indicates that the glucose-oxygen metabolic balance is shifted toward a slower mitochondrial oxidative phosphorylation, leading to a lack of ATP production capacity in the aging brain.

Interestingly, we have reported that the *in vivo* ^{31}P MRS NAD assay could also be employed at relatively lower field. Similar performance at 7T can be achieved at 4T with incorporation of ^{1}H decoupling into the ^{31}P NAD assay (Zhu et al., 2015b; Lu et al., 2016a). The advanced NAD assay approach at 4T significantly improves the spectral resolution and the SNR of the NAD^+, NADH and α-ATP (**Figures 10A,B**) owing to the proximity of the nearby protons (**Figure 10C**); excellent model fittings (**Figure 10D**) and identical RX_{NAD} value (5.3 ± 0.4, N = 7, age: 23 ± 4 years) as that of 7T (5.4 ± 0.8, N = 7, age 23 ± 2 years) were obtained (Zhu et al., 2015b; Lu et al., 2016a). This result confirms the potential of *in vivo* NAD assay for translational applications at the field strength of clinical scanners, for instance, at 3T.

In summary, the advanced *in vivo* X-nuclear MRS imaging techniques as reviewed in this article can provide quantitative measures of key physiological parameters representing metabolite contents, tissue properties and metabolic rates involving major energetic pathways in live brains. The multi-nuclear MRS imaging measurements can benefit substantially from the high/ultrahigh magnetic field for improving sensitivity

and reliability, and thus, these valuable metabolic imaging tools can be used to noninvasively assess the brain energetic changes in aging and neurodegenerative diseases. Although the neuroenergetic measurements and the quantitative markers described herein have shown feasibility and great potential in early detection of abnormal cerebral metabolism related to aging and neurodegeneration, their use in clinical practice still requires time and more efforts; nevertheless, the FDA approval of the 7T human scanner for clinical diagnosis of brain diseases will speed up the process. The same imaging methods are also suitable for studying the physiological functions and aging dependence of other organs such as the heart and skeletal muscle.

AUTHOR CONTRIBUTIONS

X-HZ and WC made equal contribution for writing and editing this review article.

REFERENCES

Ackerman, J. J. H., Grove, T. H., Wong, G. G., Gadian, D. G., and Radda, G. K. (1980). Mapping of metabolites in whole animals by ^{31}P NMR using surface coils. *Nature* 283, 167–170. doi: 10.1038/283167a0

Arai, T., Nakao, S., Morikawa, S., Inubushi, T., Yokoi, T., Shimizu, K., et al. (1998). Measurement of local cerebral blood flow by magnetic resonance imaging: *in vivo* autoradiographic strategy using ^{17}O-labeled water. *Brain Res. Bull.* 45, 451–456. doi: 10.1016/s0361-9230(97)00369-9

Atkinson, I. C., and Thulborn, K. R. (2010). Feasibility of mapping the tissue mass corrected bioscale of cerebral metabolic rate of oxygen consumption using 17-oxygen and 23-sodium MR imaging in a human brain at 9.4 T. *Neuroimage* 51, 723–733. doi: 10.1016/j.neuroimage.2010.02.056

Attwell, D., and Laughlin, S. B. (2001). An energy budget for signaling in the grey matter of the brain. *J. Cereb. Blood Flow Metab.* 21, 1133–1145. doi: 10.1097/00004647-200110000-00001

Balaban, R. S., Nemoto, S., and Finkel, T. (2005). Mitochondria, oxidants, and aging. *Cell* 120, 483–495. doi: 10.1016/j.cell.2005.02.001

Barinaga, M. (1997). What makes brain neurons run. *Science* 276, 196–198. doi: 10.1126/science.276.5310.196

Borghammer, P., Chakravarty, M., Jonsdottir, K. Y., Sato, N., Matsuda, H., Ito, K., et al. (2010). Cortical hypometabolism and hypoperfusion in Parkinson's disease is extensive: probably even at early disease stages. *Brain Struct. Funct.* 214, 303–317. doi: 10.1007/s00429-010-0246-0

Boumezbeur, F., Mason, G. F., de Graaf, R. A., Behar, K. L., Cline, G. W., Shulman, G. I., et al. (2010). Altered brain mitochondrial metabolism in healthy aging as assessed by *in vivo* magnetic resonance spectroscopy. *J. Cereb. Blood Flow Metab.* 30, 211–221. doi: 10.1038/jcbfm.2009.197

Boyer, P. D. (1999). What makes ATP synthase spin? *Nature* 402, 247–249. doi: 10.1038/46193

Braidy, N., Guillemin, G., and Grant, R. (2008). Promotion of cellular NAD^+ anabolism: therapeutic potential for oxidative stress in ageing and Alzheimer's disease. *Neurotox. Res.* 13, 173–184. doi: 10.1007/bf03033501

Braidy, N., Guillemin, G. J., Mansour, H., Chan-Ling, T., Poljak, A., and Grant, R. (2011). Age related changes in NAD^+ metabolism oxidative stress and Sirt1 activity in wistar rats. *PLoS One* 6:e19194. doi: 10.1371/journal.pone.0019194

Brooks, D. J., and Pavese, N. (2011). Imaging biomarkers in Parkinson's disease. *Prog. Neurobiol.* 95, 614–628. doi: 10.1016/j.pneurobio.2011.08.009

Chance, B., Cohen, P., Jobsis, F., and Schoener, B. (1962). Intracellular oxidation-reduction states *in vivo*: the microfluorometry of pyridine nucleotide gives a continuous measurement of the oxidation state. *Science* 137, 499–508. doi: 10.1126/science.137.3529.499

Chen, W., and Zhu, X. H. (2005). Dynamic study of cerebral bioenergetics and brain function using *in vivo* multinuclear MRS approaches. *Concepts Magn. Reson.* 27, 84–121. doi: 10.1002/cmr.a.20046

Creasey, H., and Rapoport, S. I. (1985). The aging human brain. *Ann. Neurol.* 17, 2–10. doi: 10.1002/ana.410170103

De Santi, S., de Leon, M. J., Convit, A., Tarshish, C., Rusinek, H., Tsui, W. H., et al. (1995). Age-related changes in brain: II. Positron emission tomography of frontal and temporal lobe glucose metabolism in normal subjects. *Psychiatr. Q.* 66, 357–370. doi: 10.1007/bf02238755

Du, F., Zhu, X. H., Qiao, H., Zhang, X., and Chen, W. (2007). Efficient *in vivo* ^{31}P magnetization transfer approach for noninvasively determining multiple kinetic parameters and metabolic fluxes of ATP metabolism in the human brain. *Magn. Reson. Med.* 57, 103–114. doi: 10.1002/mrm.21107

Du, F., Zhu, X. H., Zhang, Y., Friedman, M., Zhang, N., Uğurbil, K., et al. (2008). Tightly coupled brain activity and cerebral ATP metabolic rate. *Proc. Natl. Acad. Sci. U S A* 105, 6409–6414. doi: 10.1073/pnas.0710766105

Duara, R., Grady, C., Haxby, J., Ingvar, D., Sokoloff, L., Margolin, R. A., et al. (1984). Human brain glucose utilization and cognitive function in relation to age. *Ann. Neurol.* 16, 703–713. doi: 10.1002/ana.410160613

Duara, R., Margolin, R. A., Robertson-Tchabo, E. A., London, E. D., Schwartz, M., Renfrew, J. W., et al. (1983). Cerebral glucose utilization, as measured with positron emission tomography in 21 resting healthy men between the ages of 21 and 83 years. *Brain* 106, 761–775. doi: 10.1093/brain/106.3.761

Erecińska, M., and Silver, I. A. (1989). ATP and brain function. *J. Cereb. Blood Flow Metab.* 9, 2–19. doi: 10.1038/jcbfm.1989.2

Fang, E. F., Lautrup, S., Hou, Y., Demarest, T. G., Croteau, D. L., Mattson, M. P., et al. (2017). NAD^+ in aging: molecular mechanisms and translational implications. *Trends Mol. Med.* 23, 899–916. doi: 10.1016/j.molmed.2017.08.001

Ferrándiz, M. L., Martínez, M., De Juan, E., Díez, A., Bustos, G., and Miquel, J. (1994). Impairment of mitochondrial oxidative phosphorylation in the brain of aged mice. *Brain Res.* 644, 335–338. doi: 10.1016/0006-8993(94)91699-3

Fiat, D., and Kang, S. (1992). Determination of the rate of cerebral oxygen consumption and regional cerebral blood flow by non-invasive ^{17}O *in vivo* NMR spectroscopy and magnetic resonance imaging: Part 1. Theory and data analysis methods. *Neurol. Res.* 14, 303–311. doi: 10.1080/01616412.1992.11740074

Fiat, D., and Kang, S. (1993). Determination of the rate of cerebral oxygen consumption and regional cerebral blood flow by non-invasive ^{17}O *in vivo* NMR spectroscopy and magnetic resonance imaging. Part 2. Determination of $CMRO_2$ for the rat by ^{17}O NMR and $CMRO_2$, rCBF and the partition coefficient for the cat by ^{17}O MRI. *Neurol. Res.* 15, 7–22. doi: 10.1080/01616412.1993.11740100

Frosén, S., and Hoffman, R. A. (1963). Study of moderately rapid chemical exchange by means of nuclear magnetic double resonance. *J. Chem. Phys.* 39, 2892–2901. doi: 10.1063/1.1734121

Goyal, M. S., Vlassenko, A. G., Blazey, T. M., Su, Y., Couture, L. E., Durbin, T. J., et al. (2017). Loss of brain aerobic glycolysis in normal human aging. *Cell Metab.* 26, 353.e3–360.e3. doi: 10.1016/j.cmet.2017.07.010

FUNDING

The work reviewed in this article was partly supported by National Institutes of Health (NIH) grants of R01 NS041262, NS057560, NS070839 and MH111413, R24 MH106049, P41 EB015894, P30 NS5076408; the W.M. Keck Foundation.

ACKNOWLEDGMENTS

The authors thank Drs. Ming Lu, Byeong-Yeul Lee, Fei Du, Nanyin Zhang, Xiaoliang Zhang, Hao Lei, Gregor Adriany, Kamil Uğurbil, Yi Zhang and Mr. Hannes Wiesner, for their support, technical assistance and contribution to the development of the *in vivo* MRS imaging technologies as described in this review article. This article is also to commemorate Dr. Ming Lu for his seminal contributions to science and technology development.

Gruetter, R., Adriany, G., Choi, I. Y., Henry, P. G., Lei, H. X., and Oz, G. L. (2003). Localized *in vivo* C-13 NMR spectroscopy of the brain. *NMR Biomed.* 16, 313–338. doi: 10.1002/nbm.841

Guarente, L. (2008). Mitochondria—a nexus for aging, calorie restriction, and sirtuins? *Cell* 132, 171–176. doi: 10.1016/j.cell.2008.01.007

Guarente, L. (2016). CELL METABOLISM. The resurgence of NAD^+. *Science* 352, 1396–1397. doi: 10.1126/science.aag1718

Hetherington, H. P., Pan, J. W., and Spencer, D. D. (2002). ^1H and ^{31}P spectroscopy and bioenergetics in the lateralization of seizures in temporal lobe epilepsy. *J. Magn. Reson. Imaging* 16, 477–483. doi: 10.1002/jmri.10177

Hyder, F., Patel, A. B., Gjedde, A., Rothman, D. L., Behar, K. L., and Shulman, R. G. (2006). Neuronal-glial glucose oxidation and glutamatergic-GABAergic function. *J. Cereb. Blood Flow Metab.* 26, 865–877. doi: 10.1038/sj.jcbfm.9600263

Imai, S., and Guarente, L. (2014). NAD^+ and sirtuins in aging and disease. *Trends Cell Biol.* 24, 464–471. doi: 10.1016/j.tcb.2014.04.002

Kemp, G. J. (2000). Non-invasive methods for studying brain energy metabolism: what they show and what it means. *Dev. Neurosci.* 22, 418–428. doi: 10.1159/000017471

Kurzhunov, D., Borowiak, R., Reisert, M., Joachim Krafft, A., Caglar Özen, A., and Bock, M. (2017). 3D $CMRO_2$ mapping in human brain with direct ^{17}O MRI: comparison of conventional and proton-constrained reconstructions. *Neuroimage* 155, 612–624. doi: 10.1016/j.neuroimage.2017.05.029

Leenders, K. L., Perani, D., Lammertsma, A. A., Heather, J. D., Buckingham, P., Healy, M. J., et al. (1990). Cerebral blood flow, blood volume and oxygen utilization. Normal values and effect of age. *Brain* 113, 27–47. doi: 10.1093/brain/113.1.27

Lei, H., Uğurbil, K., and Chen, W. (2003a). Measurement of unidirectional Pi to ATP flux in human visual cortex at 7 Tesla using *in vivo* ^{31}P magnetic resonance spectroscopy. *Proc. Natl. Acad. Sci. U S A* 100, 14409–14414. doi: 10.1073/pnas.2332656100

Lei, H., Zhu, X. H., Zhang, X. L., Uğurbil, K., and Chen, W. (2003b). *In vivo* ^{31}P magnetic resonance spectroscopy of human brain at 7 T: an initial experience. *Magn. Reson. Med.* 49, 199–205. doi: 10.1002/mrm.10379

Lenzi, G. L., Jones, T., and Frackowiak, R. S. (1981). Positron emission tomography: state of the art in neurology. *Prog. Nucl. Med.* 7, 118–137.

Lin, A. L., Coman, D., Jiang, L., Rothman, D. L., and Hyder, F. (2014). Caloric restriction impedes age-related decline of mitochondrial function and neuronal activity. *J. Cereb. Blood Flow Metab.* 34, 1440–1443. doi: 10.1038/jcbfm.2014.114

López-Otín, C., Blasco, M. A., Partridge, L., Serrano, M., and Kroemer, G. (2013). The hallmarks of aging. *Cell* 153, 1194–1217. doi: 10.1016/j.cell.2013.05.039

Lu, M., Chen, W., and Zhu, X. H. (2014a). Field dependence study of *in vivo* brain ^{31}P MRS up to 16.4 T. *NMR Biomed.* 27, 1135–1141. doi: 10.1002/nbm.3167

Lu, M., Zhu, X. H., Zhang, Y., and Chen, W. (2014b). Intracellular redox state revealed by *in vivo* ^{31}P MRS measurement of NAD^+ and NADH contents in brains. *Magn. Reson. Med.* 71, 1959–1972. doi: 10.1002/mrm.24859

Lu, M., Zhang, Y., Uğurbil, K., Chen, W., and Zhu, X. H. (2013). *In vitro* and *in vivo* studies of ^{17}O NMR sensitivity at 9.4 and 16.4 T. *Magn. Reson. Med.* 69, 1523–1527. doi: 10.1002/mrm.24386

Lu, M., Zhu, X. H., and Chen, W. (2016a). *In vivo* ^{31}P MRS assessment of intracellular NAD metabolites and NAD^+/NADH redox state in human brain at 4 T. *NMR Biomed.* 29, 1010–1017. doi: 10.1002/nbm.3559

Lu, M., Zhu, X. H., Zhang, Y., Low, W., and Chen, W. (2016b). "Simultaneous assessment of abnormal glycolysis and oxidative metabolisms in brain tumor using *in vivo* deuterium (^2H) MRS imaging," in *Proceedings of the International Society for Magnetic Resonance in Medicine* (Singapore), 3962.

Lu, M., Zhu, X. H., Zhang, Y., and Chen, W. (2018). "A pilot study for *in vivo* measurement and quantification of brain glucose metabolic rates using oral uptake of deuterated glucose," in *Proceedings of the International Society for Magnetic Resonance in Medicine* (Paris, France), 907.

Lu, M., Zhu, X. H., Zhang, Y., Mateescu, G., and Chen, W. (2017). Quantitative assessment of brain glucose metabolic rates using *in vivo* deuterium magnetic resonance spectroscopy. *J. Cereb. Blood Flow Metab.* 37, 3518–3530. doi: 10.1177/0271678x17706444

Marchal, G., Rioux, P., Petit-Taboué, M. C., Sette, G., Travère, J. M., Le Poec, C., et al. (1992). Regional cerebral oxygen consumption, blood flow, and blood volume in healthy human aging. *Arch. Neurol.* 49, 1013–1020. doi: 10.1001/archneur.1992.00530340029014

Mateescu, G. D., Ye, A., Flask, C. A., Erokwu, B., and Duerk, J. L. (2011). *In vivo* assessment of oxygen consumption via deuterium magnetic resonance. *Adv. Exp. Med. Biol.* 701, 193–199. doi: 10.1007/978-1-4419-7756-4_26

Mateescu, G. D., Yvars, G., Pazara, D. I., Alldridge, N. A., Lamanna, J. C., Lust, D. W., et al. (1989). "^{17}O-^1H magnetic resonance imaging in plants, animals, and materials," in *Synthesis and Application of Isotopically Labeled Compounds*, eds T. A. Baillie and J. R. Jones (Amsterdam: Elsevier), 499–508.

Mills, K. F., Yoshida, S., Stein, L. R., Grozio, A., Kubota, S., Sasaki, Y., et al. (2016). Long-term administration of nicotinamide mononucleotide mitigates age-associated physiological decline in mice. *Cell Metab.* 24, 795–806. doi: 10.1016/j.cmet.2016.09.013

Mintun, M. A., Raichle, M. E., Martin, W. R., and Herscovitch, P. (1984). Brain oxygen utilization measured with O-15 radiotracers and positron emission tomography. *J. Nucl. Med.* 25, 177–187.

Mouchiroud, L., Houtkooper, R. H., and Auwerx, J. (2013). NAD^+ metabolism: a therapeutic target for age-related metabolic disease. *Crit. Rev. Biochem. Mol. Biol.* 48, 397–408. doi: 10.3109/10409238.2013

Navarro, A., and Boveris, A. (2007). The mitochondrial energy transduction system and the aging process. *Am. J. Physiol. Cell Physiol.* 292, C670–C686. doi: 10.1152/ajpcell.00213.2006

Niccolini, F., Su, P., and Politis, M. (2014). Dopamine receptor mapping with PET imaging in Parkinson's disease. *J. Neurol.* 261, 2251–2263. doi: 10.1007/s00415-014-7302-2

Niesporek, S. C., Umathum, R., Lommen, J. M., Behl, N. G. R., Paech, D., Bachert, P., et al. (2018). Reproducibility of $CMRO_2$ determination using dynamic ^{17}O MRI. *Magn. Reson. Med.* 79, 2923–2934. doi: 10.1002/mrm.26952

Nunnari, J., and Suomalainen, A. (2012). Mitochondria: in sickness and in health. *Cell* 148, 1145–1159. doi: 10.1016/j.cell.2012.02.035

Pantano, P., Baron, J. C., Lebrun-Grandie, P., Duquesnoy, N., Bousser, M. G., and Comar, D. (1984). Regional cerebral blood flow and oxygen consumption in human aging. *Stroke* 15, 635–641. doi: 10.1161/01.STR.15.4.635

Pathak, D., Berthet, A., and Nakamura, K. (2013). Energy failure: does it contribute to neurodegeneration? *Ann. Neurol.* 74, 506–516. doi: 10.1002/ana.24014

Pekar, J., Ligeti, L., Ruttner, Z., Lyon, R. C., Sinnwell, T. M., van Gelderen, P., et al. (1991). *In vivo* measurement of cerebral oxygen consumption and blood flow using ^{17}O magnetic resonance imaging. *Magn. Reson. Med.* 21, 313–319. doi: 10.1002/mrm.1910210217

Qiao, H., Zhang, X., Zhu, X. H., Du, F., and Chen, W. (2006). *In vivo* ^{31}P MRS of human brain at high/ultrahigh fields: a quantitative comparison of NMR detection sensitivity and spectral resolution between 4 T and 7 T. *Magn. Reson. Imaging* 24, 1281–1286. doi: 10.1016/j.mri.2006.08.002

Raichle, M. E. (1987). "Circulatory and metabolic correlates of brain function in normal humans," in *Handbook of Physiology—The Nervous System*, eds V. B. Mountcastle, F. Plum and S. R. Geiger (Bethesda, MD: American Physiological Society), 643–674.

Rapoport, S. I. (1999). Functional brain imaging in the resting state and during activation in Alzheimer's disease. Implications for disease mechanisms involving oxidative phosphorylation. *Ann. N Y Acad. Sci.* 893, 138–153. doi: 10.1111/j.1749-6632.1999.tb07823.x

Reddy, P. H., and Reddy, T. P. (2011). Mitochondria as a therapeutic target for aging and neurodegenerative diseases. *Curr. Alzheimer Res.* 8, 393–409. doi: 10.2174/156720511795745401

Reddy, R., Stolpen, A. H., Charagundla, S. R., Insko, E. K., and Leigh, J. S. (1996). ^{17}O-decoupled 1H detection using a double-tuned coil. *Magn. Reson. Imaging* 14, 1073–1078. doi: 10.1016/s0730-725x(96)00227-5

Ren, J., Sherry, A. D., and Malloy, C. R. (2017). Efficient ^{31}P band inversion transfer approach for measuring creatine kinase activity, ATP synthesis, and molecular dynamics in the human brain at 7 T. *Magn. Reson. Med.* 78, 1657–1666. doi: 10.1002/mrm.26560

Rodrigues, T. B., Valette, J., and Bouzier-Sore, A.-K. (2013). 13_C NMR spectroscopy applications to brain energy metabolism. *Front. Neuroenergetics* 5:9. doi: 10.3389/fnene.2013.00009

Rolfe, D. F., and Brown, G. C. (1997). Cellular energy utilization and molecular origin of standard metabolic rate in mammals. *Physiol. Rev.* 77, 731–758. doi: 10.1152/physrev.1997.77.3.731

Ronen, I., Merkle, H., Uğurbil, K., and Navon, G. (1998). Imaging of $H_2{}^{17}O$ distribution in the brain of a live rat by using proton-detected ^{17}O MRI. *Proc. Natl. Acad. Sci. U S A* 95, 12934–12939. doi: 10.1073/pnas.95.22.12934

Rothman, D. L., De Feyter, H. M., de Graaf, R. A., Mason, G. F., and Behar, K. L. (2011). 13_C MRS studies of neuroenergetics and neurotransmitter cycling in humans. *NMR Biomed.* 24, 943–957. doi: 10.1002/nbm.1772

Schägger, H., and Ohm, T. G. (1995). Human diseases with defects in oxidative phosphorylation. 2. F_1F_0 ATP-synthase defects in Alzheimer disease revealed by blue native polyacrylamide gel electrophoresis. *Eur. J. Biochem.* 227, 916–921. doi: 10.1111/j.1432-1033.1995.tb20219.x

Schultz, M. B., and Sinclair, D. A. (2016). Why NAD^+ declines during aging: it's destroyed. *Cell Metab.* 23, 965–966. doi: 10.1016/j.cmet.2016.05.022

Shoubridge, E. A., Briggs, R. W., and Radda, G. K. (1982). ^{31}P NMR saturation transfer measurements of the steady state rates of creatine kinase and ATP synthetase in the rat brain. *FEBS Lett.* 140, 288–292. doi: 10.1016/0014-5793(82)80916-2

Shulman, R. G., Brown, T. R., Uğurbil, K., Ogawa, S., Cohen, S. M., and Den Hollander, J. A. (1979). Cellular applications of ^{31}P and ^{13}C nuclear magnetic resonance. *Science* 205, 160–166. doi: 10.1126/science.36664

Shulman, R. G., Rothman, D. L., Behar, K. L., and Hyder, F. (2004). Energetic basis of brain activity: implications for neuroimaging. *Trends Neurosci.* 27, 489–495. doi: 10.1016/j.tins.2004.06.005

Shulman, R. G., Rothman, D. L., and Hyder, F. (1999). Stimulated changes in localized cerebral energy consumption under anesthesia. *Proc. Natl. Acad. Sci. U S A* 96, 3245–3250. doi: 10.1073/pnas.96.6.3245

Sibson, N. R., Mason, G. F., Shen, J., Cline, G. W., Herskovits, A. Z., Wall, J. E., et al. (2001). *In vivo* ^{13}C NMR measurement of neurotransmitter glutamate cycling, anaplerosis and TCA cycle flux in rat brain during. *J. Neurochem.* 76, 975–989. doi: 10.1046/j.1471-4159.2001.00074.x

Siesjo, B. K. (1978). *Brain Energy Metabolism*. New York, NY: Wiley.

Sonnay, S., Gruetter, R., and Duarte, J. M. N. (2017). How energy metabolism supports cerebral function: insights from 13_C magnetic resonance studies *In vivo*. *Front. Neurosci.* 11:288. doi: 10.3389/fnins.2017.00288

Stryer, L. (1988). *Biochemistry.* New York, NY: W.H. Freeman & Company.

Uğurbil, K. (1985). Magnetization transfer measurements of individual rate constants in the presence of multiple reactions. *J. Magn. Reson.* 64, 207–219. doi: 10.1016/0022-2364(85)90345-2

Varley, J., Brooks, D. J., and Edison, P. (2015). Imaging neuroinflammation in Alzheimer's and other dementias: recent advances and future directions. *Alzheimers Dement.* 11, 1110–1120. doi: 10.1016/j.jalz.2014.08.105

Vaughan, J. T., Garwood, M., Collins, C. M., Liu, W., Delabarre, L., Adriany, G., et al. (2001). 7T vs. 4T: RF power, homogeneity, and signal-to-noise comparison in head images. *Magn. Reson. Med.* 46, 24–30. doi: 10.1002/mrm.1156

Verdin, E. (2015). NAD^+ in aging, metabolism, and neurodegeneration. *Science* 350, 1208–1213. doi: 10.1126/science.aac4854

Wu, M. F., Yin, J. H., Hwang, C. S., Tang, C. M., and Yang, D. I. (2014). NAD attenuates oxidative DNA damages induced by amyloid β-peptide in primary rat cortical neurons. *Free Radic. Res.* 48, 794–805. doi: 10.3109/10715762.2014.907889

Xie, W. J., Xu, A. S., and Yeung, E. S. (2009). Determination of NAD^+ and NADH in a single cell under hydrogen peroxide stress by capillary electrophoresis. *Anal. Chem.* 81, 1280–1284. doi: 10.1021/ac802249m

Yamaguchi, T., Kanno, I., Uemura, K., Shishido, F., Inugami, A., Ogawa, T., et al. (1986). Reduction in regional cerebral metabolic rate of oxygen during human aging. *Stroke* 17, 1220–1228. doi: 10.1161/01.str.17.6.1220

Yang, H. Y., Yang, T., Baur, J. A., Perez, E., Matsui, T., Carmona, J. J., et al. (2007). Nutrient-sensitive mitochondrial NAD^+ levels dictate cell survival. *Cell* 130, 1095–1107. doi: 10.1016/j.cell.2007.07.035

Yap, L. P., Garcia, J. V., Han, D., and Cadenas, E. (2009). The energy-redox axis in aging and age-related neurodegeneration. *Adv. Drug Deliv. Rev.* 61, 1283–1298. doi: 10.1016/j.addr.2009.07.015

Yin, F., Boveris, A., and Cadenas, E. (2014). Mitochondrial energy metabolism and redox signaling in brain aging and neurodegeneration. *Antioxid. Redox Signal.* 20, 353–371. doi: 10.1089/ars.2012.4774

Ying, W. H. (2007). NAD^+ and NADH in brain functions, brain diseases and brain aging. *Front. Biosci.* 12, 1863–1888. doi: 10.2741/2194

Zhang, Q. H., Wang, S. Y., Nottke, A. C., Rocheleau, J. V., Piston, D. W., and Goodman, R. H. (2006). Redox sensor CtBP mediates hypoxia-induced tumor cell migration. *Proc. Natl. Acad. Sci. U S A* 103, 9029–9033. doi: 10.1073/pnas.0603269103

Zhang, N., Zhu, X. H., Lei, H., Uğurbil, K., and Chen, W. (2004). Simplified methods for calculating cerebral metabolic rate of oxygen based on ^{17}O magnetic resonance spectroscopic imaging measurement during a short $^{17}O_2$ inhalation. *J. Cereb. Blood Flow Metab.* 24, 840–848. doi: 10.1097/01.WCB.0000125885.54676.82

Zhu, X. H., and Chen, W. (2011). *In vivo* oxygen-17 NMR for imaging brain oxygen metabolism at high field. *Prog. Nucl. Magn Reson. Spectrosc.* 59, 319–335. doi: 10.1016/j.pnmrs.2011.04.002

Zhu, X. H., Chen, J. M., Tu, T. W., Chen, W., and Song, S. K. (2013a). Simultaneous and noninvasive imaging of cerebral oxygen metabolic rate, blood flow and oxygen extraction fraction in stroke mice. *Neuroimage* 64, 437–447. doi: 10.1016/j.neuroimage.2012.09.028

Zhu, X. H., Zhang, Y., Wiesner, H. M., Uğurbil, K., and Chen, W. (2013b). *In vivo* measurement of CBF using ^{17}O NMR signal of metabolically produced $H_2{}^{17}O$ as a perfusion tracer. *Magn. Reson. Med.* 70, 309–314. doi: 10.1002/mrm.24469

Zhu, X. H., Du, F., Zhang, N., Lu, M., Zhang, Y., Liu, X., et al. (2015a). *Study of Brain Bioenergetics and Function Using In Vivo MRS*. New York, NY: Springer.

Zhu, X. H., Lu, M., Lee, B. Y., Uğurbil, K., and Chen, W. (2015b). *In Vivo* NAD assay reveals the intracellular NAD contents and redox state in healthy human brain and their age dependences. *Proc. Natl. Acad. Sci. U S A* 112, 2876–2881. doi: 10.1073/pnas.1417921112

Zhu, X. H., Lee, B. Y., and Chen, W. (2018). Functional energetic responses and individual variance of the human brain revealed by quantitative imaging of adenosine triphosphate production rates. *J. Cereb. Blood Flow Metab.* 38, 959–972. doi: 10.1177/0271678x18769039

Zhu, X. H., Liu, X., Lu, M., Wiesner, H. M., Uğurbil, K., and Chen, W. (2014). "*In vivo* ^{17}O MR imaging and quantification of $CMRO_2$, CBF and OEF in human visual cortex at rest and during activation," in *Proceedings of the International Society for Magnetic Resonance in Medicine* (Milan, Italy), 3763.

Zhu, X. H., Merkle, H., Kwag, J. H., Uğurbil, K., and Chen, W. (2001). ^{17}O relaxation time and NMR sensitivity of cerebral water and their field dependence. *Magn. Reson. Med.* 45, 543–549. doi: 10.1002/mrm.1073

Zhu, X. H., Qiao, H., Du, F., Xiong, Q., Liu, X., Zhang, X., et al. (2012). Quantitative imaging of energy expenditure in human brain. *Neuroimage* 60, 2107–2117. doi: 10.1016/j.neuroimage.2012.02.013

Zhu, X. H., Zhang, Y., Tian, R. X., Lei, H., Zhang, N., Zhang, X., et al. (2002). Development of ^{17}O NMR approach for fast imaging of cerebral metabolic rate of oxygen in rat brain at high field. *Proc. Natl. Acad. Sci. U S A* 99, 13194–13199. doi: 10.1073/pnas.202471399

Zhu, X. H., Zhang, Y., Zhang, N., Uğurbil, K., and Chen, W. (2007). Noninvasive and three-dimensional imaging of $CMRO_2$ in rats at 9.4 T: reproducibility test and normothermia/hypothermia comparison study. *J. Cereb. Blood Flow Metab.* 27, 1225–1234. doi: 10.1038/sj.jcbfm.9600421

Zhu, X. H., Zhang, N., Zhang, Y., Uğurbil, K., and Chen, W. (2009). New insights into central roles of cerebral oxygen metabolism in the resting and stimulus-evoked brain. *J. Cereb. Blood Flow Metab.* 29, 10–18. doi: 10.1038/jcbfm.2008.97

Zhu, X. H., Zhang, N., Zhang, Y., Zhang, X., Uğurbil, K., and Chen, W. (2005). *In vivo* ^{17}O NMR approaches for brain study at high field. *NMR Biomed.* 18, 83–103. doi: 10.1002/nbm.930

Conflict of Interest Statement: The authors declare that the research was conducted in the absence of any commercial or financial relationships that could be construed as a potential conflict of interest.